Mimicking an Atomically Thin "Vacuum Spacer" to Measure the Hamaker Constant between Graphene Oxide and Silica

Chu, Liangyong; Korobko, A.V.; Cao, Anping; Sachdeva, Sumit; Liu, Zhen; de Smet, Louis C P M; Sudholter, E.J.R.; Picken, Stephen J.; Besseling, Nicolaas A M

DOI
10.1002/admi.201600495

Publication date
2017

Document Version
Final published version

Published in
Advanced Materials Interfaces

ADVANCED MATERIALS INTERFACES
www.advmatinterfaces.de

Mimicking an Atomically Thin "Vacuum Spacer" to Measure the Hamaker Constant between Graphene Oxide and Silica

*Liangyong Chu, Alexander V. Korobko, Anping Cao, Sumit Sachdeva, Zhen Liu, Louis C. P. M. de Smet, Ernst J. R. Sudhölter, Stephen J. Picken, and Nicolaas A. M. Besseling**

In nanoscience, control of the separation between surfaces, with sub-nm accuracy, is often important. For instance, when studying van der Waals (vdW) forces[1] or creating nanogaps for molecule detection and separation.[2] At nanometer scales, 1D or 3D spacers, such as nanotubes and nanoparticles, are susceptible to deformation.[3] A 2D spacer is expected to yield a more accurately defined separation, owing to the high atom density and strength in planar direction. Herein, atomically thin 2D graphene oxide (GO) was used as nanometer-scale spacer with sub-nm accuracy, to study vdW interactions. However, using such a physical spacer introduces additional interactions, obscuring the interactions of interest. We demonstrate how these contributions can be eliminated by effectively mimicking the use of a "vacuum spacer." In this way, we obtain the effective Hamaker constant between GO and silica.

Following the excitement about graphene, GO is drawing more and more attention.[4] Using GO as a precursor, many graphene derivatives and heterostructures[1] have been made, and used in various areas such as composites,[5] energy storage, and conversion,[6] bioscience, mechanical, and electronic devices and sensors.[7]

In all these applications, graphene-based materials are used in combination with other materials. Hence, the relevance of interfacial forces such as vdW,[1,8] capillary,[9] and electrostatic[10] forces. The vdW forces, which are always present, can be quantified by the so-called Hamaker constant.[11] The unretarded vdW interaction energy $U_{vdW}(d)$ between two material surfaces is[11,12]

$$U_{vdW}(d) = -A_{12}/12\pi d^2 \quad (1)$$

where d is the separation distance, and A_{12} is the Hamaker constant.

Knowing the Hamaker constant between graphene-based materials and other materials (e.g., silicon (Si) with native silica layer as used in electronic devices) is important for their application, but measuring this constant is challenging. According to Equation (1), to determine the Hamaker constant, the vdW interaction energy needs to be determined for a known separation distance. Several investigations have been made to establish the strength of vdW interactions between graphene and Si by measuring the adhesion energy.[13] However, the effective distance between a graphene sheet and a Si surface could not be determined precisely in these experiments. The effective separation distance of two "touching" surfaces varies from 1 to 2 Å depending on the surface roughness.[14] At small separation distances, the limited accuracy of the distance measurement (typical error of 1 nm) leads to a huge error in the calculated value of the Hamaker constant according to Equation (1). In principle, this problem could be solved by a spacer with a precisely known thickness of about 1 nm. At such distances, the magnitude of the vdW energy is sufficient for accurate measurement, and the retardation effect is unimportant.[15] The ideal spacer would be one that "consists of vacuum," so that it would not contribute to the interactions.

Capillary[9] and electrostatic[10] forces complicate determination of the vdW energy even further.

Figure 1 illustrates the experiment that mimics the application of a vacuum spacer in an atomic force microscopy (AFM) force measurement, by measuring the adhesion force between an AFM tip and both mono- and bilayers of GO on an Si/polymer substrate. From the difference between the measured adhesion force on GO monolayer and on GO bilayer (Figure 1a,b, respectively), capillary and electrostatic forces, and the vdW interactions between tip and underlying substrate cancel. Hence, we obtain the interaction force between a levitating GO nanosheet and the AFM tip, at a distance d corresponding to the thickness of the GO top layer, as if they were separated by a vacuum spacer with a thickness equal to that of the intervening GO top layer.

Sample preparation and morphology of the Si/poly-ethyleneimine (PEI)/GO structures depicted in Figure 1a,b are summarized and illustrated in **Figure 2**, and described in the sample preparation section.

The surface morphology of the Si/PEI/GO sample as drawn in Figure 2c.5, was characterized using HybriD Mode AFM, by which we obtain simultaneously a height image and an adhesive-force image (for details see the Instrumentation and methods part in the Experimental Section). **Figure 3** shows results collected at different locations of the same sample. Height images are shown in Figure 3a,d. GO flakes are recognizable by their larger height, by about 5 nm, relative to the silicon. This 5 nm represents the combined thickness of GO and underlying PEI. Features in the adhesion-force image coincide with features in the height counterpart. However, inspection

L. Chu, Dr. A. V. Korobko, A. Cao, S. Sachdeva, Dr. Z. Liu, Dr. L. C. P. M. de Smet, Prof. E. J. R. Sudhölter, Prof. S. J. Picken, Dr. N. A. M. Besseling
Department of Chemical Engineering
Organic Materials & Interface (OMI)
Delft University of Technology
Julianalaan 136, 2628 BL Delft, The Netherlands
E-mail: N.A.M.Besseling@tudelft.nl

DOI: 10.1002/admi.201600495

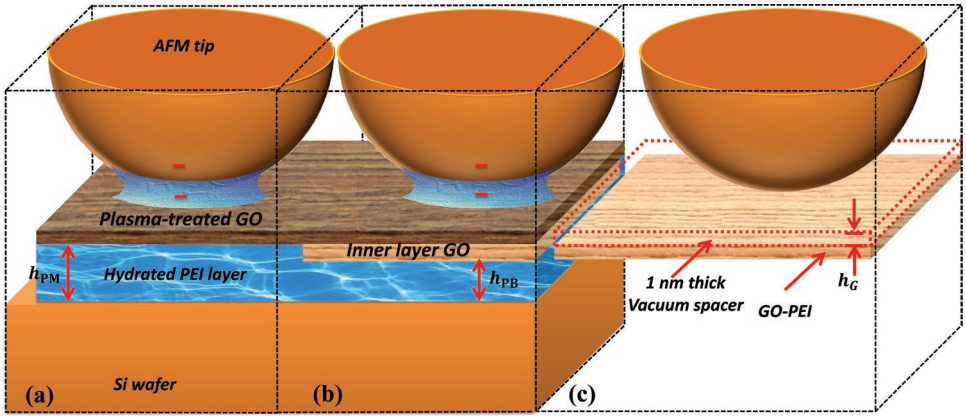

Figure 1. Schematic illustration of the experiment. a) Silicon tip in contact with Si/PEI/GO monolayer. b) Si tip in contact with Si/PEI/GO bilayer. The measured adhesion forces between the Si tip and the Si/PEI/GO layer in (a) and (b) are due to vdW forces, capillary forces, electrostatic forces and specific interactions between chemical moieties such as hydrogen bonds. c) The difference between situation (a) and (b) mimics the AFM tip interacting with a GO monolayer in vacuum at a distance *d*, equal to the thickness of a GO monolayer. Capillary, electrostatic, and other forces cancel out.

of the adhesion-force image reveals features not visible in the height image. Folding and overlapping of GO, which forms a bilayer at some places, causes variations of the adhesion force. In adhesion-force images (Figures 2e and 3b) and profiles (Figure 3c,f) we recognize two distinct levels at the GO flakes. In Figure 3d,e we observe a straight edge, quite different from other more irregular edges of the GO flakes, which represents a fold of a flake. Adjoining this edge there must be a GO bilayer. Indeed, in the adhesion-force image (Figure 3e), and profile (Figure 3f), we clearly recognize the bilayer patch adjoining this

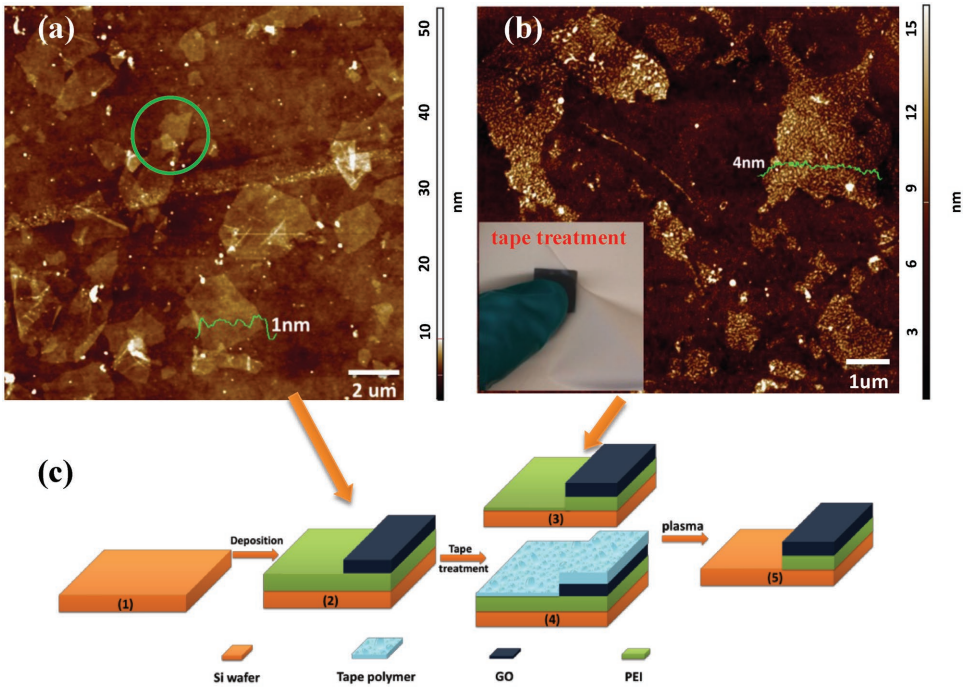

Figure 2. a) AFM height images of GO deposited on a Si/PEI surface. GO flakes are clearly visible with thickness of about 1 nm,[21] as well as areas exhibiting a twofold increase of the height. The latter is interpreted as two GO nanosheets overlapping (indicated by the green circle). b) AFM height images of the Si/PEI/GO sample after tape treatment. The inset of 2b shows the sample being pressed on the tape. c) Schematic illustration of the sample preparation. Clearly, GO flakes have remained at the sample upon the tape treatment. Their height increased to 4 nm, the heights for monolayer and bilayer sections are now the same. Furthermore, the surface roughness increased. There are two possible explanations for the increased height of the GO-covered regions: (c.3) the tape/PEI interaction is so strong that (part of) the PEI next to GO flakes was removed by the tape, and the tape/GO interaction is so much weaker that GO and PEI covered by it were not removed. (c.4) polymer molecules from the tape were left behind, and their quantity on GO was larger than that on PEI. After plasma treatment, the sample has flakes of GO with PEI underneath on Si. The area not covered by GO is simply bare Si, as illustrated in (c.5). As discussed in detail, this structure is confirmed by AFM height and force images, simultaneously obtained by the HybriD Mode method.[29]

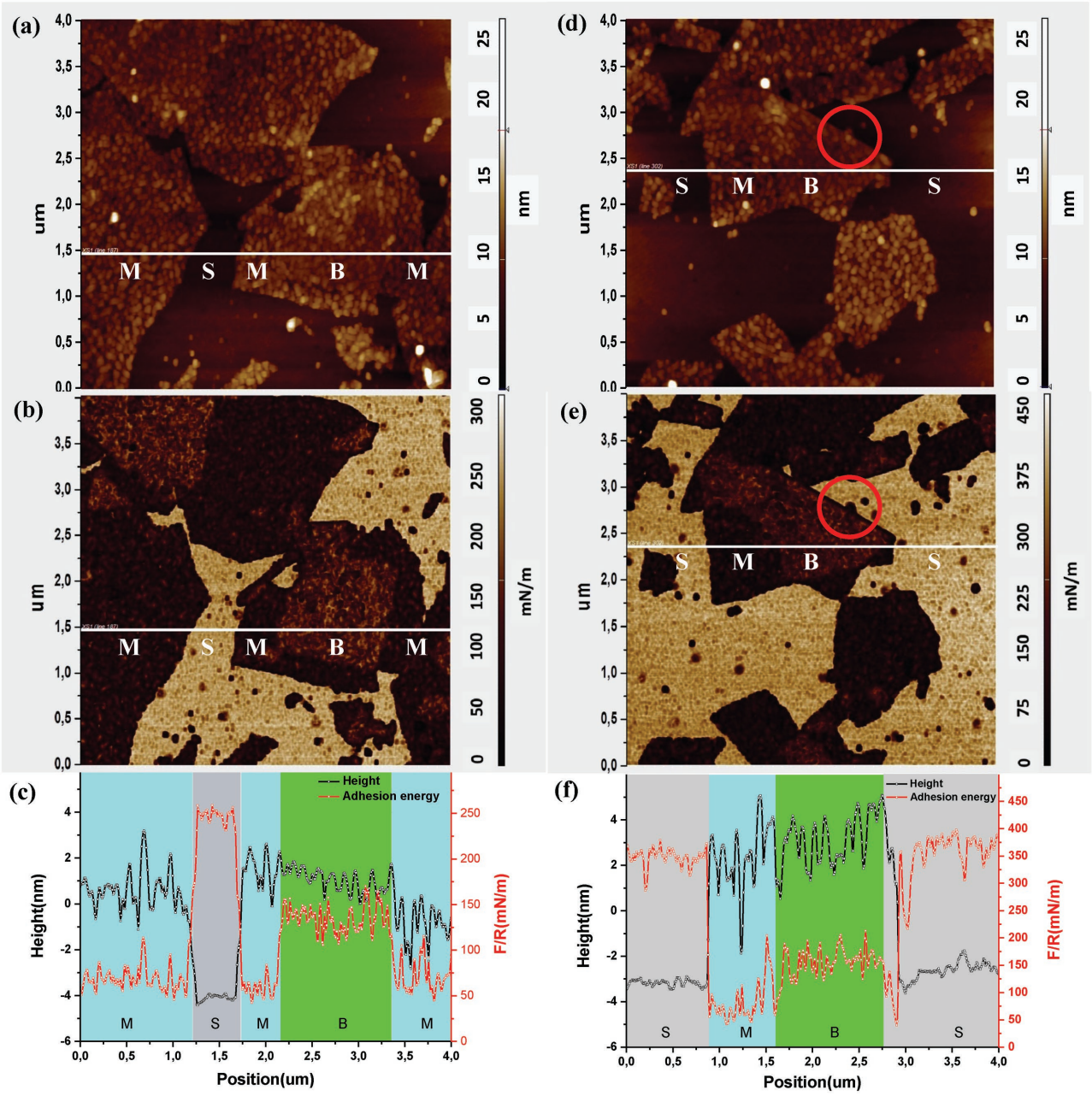

Figure 3. Surface morphology and adhesion-force images and profiles of Si/PEI/GO samples with a structure as illustrated in Figure 2c.5, obtained using HybriD Mode AFM. a) Height image. b) Normalized adhesion-force image of the same area. c) Height and normalized adhesion-force profiles along the white line indicated in (a) and (b). S marks bare Si, M marks PEI/monolayer GO on Si wafer, and B marks PEI/bilayer GO on Si wafer. Values of normalized adhesion forces averaged over 5 points at a GO monolayer and at a bilayer are $F_M/R = 76 \pm 3$ mN m^{-1} and $F_B/R = 151 \pm 4$ mN m^{-1}, respectively, and the difference between these is 75 ± 5 mN m^{-1}. (d–f) The results of a repeated experiment at a different location of the same sample using the same AFM tip are shown. These were obtained on another day, when temperature and humidity were somewhat different. Values $F_M/R = 63 \pm 2$ mN m^{-1} and $F_B/R = 136 \pm 3$ mN m^{-1} are quite different from the ones mentioned before, but the difference between these is the same within experimental accuracy (73 ± 4 mN m^{-1}). The straight edge, indicated by the red circles represents a fold of the GO flake.

fold. The bilayer is characterized by a larger adhesive energy than the monolayer patches. Also in other places (e.g., image 2.b and profile 2.c) we recognize patches with this higher-level adhesive force. After the tape treatment, both the GO monolayer and bilayer are rough. For the subsequent analysis, we selected regions on the monolayer and on the bilayer where the height is the same. This procedure is explained in detail in Section 3 of the Supporting Information. Figure 3c,f represents typical single scan profiles along the white lines in Figure 3a,b,d,e, respectively.

According to the Derjaguin approximation,[16] the interaction force F between a spherical surface of radius R (e.g., the AFM

tip) and a flat surface (e.g., the Si/PEI/GO surface) is related to the interaction energy per unit area U between two planar surfaces via

$$\frac{F}{R} = 2\pi U \tag{2}$$

This relation applies to, e.g., the vdW interactions and screened electrostatic interactions when the distance between the surfaces is considerably smaller than the radius R. It does not apply to interactions associated with capillary bridges. According to the Hamaker-de Boer approximation,[11,17] the vdW interaction energy per unit area between a planar silica surface and a Si/PEI/GO surface at a distance D, with a GO thickness h_G and a PEI thickness h_P, is described by

$$U_{vdW}(D, h_G, h_P) = -\left[\frac{A_{SG}}{12\pi}\left(\frac{1}{D^2} - \frac{1}{(D+h_G)^2}\right) + \frac{A_{SP}}{12\pi}\left(\frac{1}{(D+h_G)^2} - \frac{1}{(D+h_G+h_P)^2}\right) + \frac{A_{SSi}}{12\pi}\left(\frac{1}{(D+h_G+h_P)^2}\right) \right] \tag{3}$$

where A_{SG}, A_{SP}, A_{SSi} are the Hamaker constants of Silica/GO, Silica/PEI and Silica/Si, respectively (Section 1, Supporting Information).

The capillary force ($\frac{F}{R} \approx$, the surface tension of water)[18] has a similar order of magnitude as the measured normalized force. However, its exact value is difficult to establish as it depends on humidity and the local surface morphology. Furthermore, the electrostatic force depends on the physical and chemical properties of the surface such as the surface charge densities, which are not known.

Assuming additivity, the measured normalized force F/R is

$$F/R = 2\pi U_{vdW}(D, h_G, h_P) + F_c/R + F_e/R \tag{4}$$

where F_c and F_e represent the capillary and electrostatic forces, respectively.

It is not possible to obtain the Hamaker constant A_{SG} using separate values for F_M/R or for F_B/R as reported in Figure 3, because there are four unknown variables (A_{SG}, D, F_c, F_e). In order to obtain the Hamaker constant, the capillary and electrostatic forces have to be eliminated from analysis. Making some reasonable assumptions, it is possible to obtain the Hamaker constant from the difference between F_M/R and F_B/R. These assumptions are the additivity principle (Equation (4)), and the assumption that the electrostatic and capillary forces are the same for GO monolayers and GO bilayers. This is reasonable as these contributions are largely determined by the nature of the outer surface, which is the same for GO mono and bilayers.

The capillary force F_c in AFM force measurement can be described as,[19] $F_c = 2R(\cos\theta_1 + \cos\theta_2)$, where γ is surface tension of water, R is the radius of the AFM tip, θ_1 is the contact angle of AFM tip(silica), θ_2 is the contact angle of sample surface. The folded under layer has very limited effect on θ_2. The effect on the capillary force itself is even smaller.

The plasma treatment of the GO surfaces will probably induce some changes. However, this does not influence our final result, as the upper layer does not contribute to the final results and acts as a protecting layer for the second layer during the plasma treatment.

According to these assumptions, the normalized force for a levitating GO nanosheet positioned below the AFM tip at a distance d corresponding to the thickness of the GO top layer, equals

$$\begin{aligned} F_B/R - F_M/R &= \left[2\pi U(D, 2h_G, h_{PB}) + F_{B,c} + F_{B,e}\right] \\ &\quad - \left[2\pi U(D, h_G, h_{PM}) + F_{M,c} + F_{M,e}\right] \\ &= \frac{A_{SG} - A_{SP}}{6}\left(\frac{1}{h_G^2} - \frac{1}{(2h_G)^2}\right) = \frac{1}{8}\frac{A_{SG} - A_{SP}}{d^2} \end{aligned} \tag{5}$$

Here, the separation distance d is equal to h_G. The second equality assumes that capillary and electrostatic forces are the same for the GO mono- and bilayer, so that these cancel. This relation enables us to calculate A_{SG} from the force difference, once R, d and A_{SP} are known.

The value for $d = h_G$ is 0.89 ± 0.06 nm (Section 4, Supporting Information). The radius R of the AFM tip is 10.6 nm (Section 6, Supporting Information). To estimate A_{SP} we refer to Berthelot principle[16]

$$A_{SP} \approx (A_{SS}A_{PP})^{1/2} \tag{6}$$

For polymers such as, e.g., PEI, the Hamaker constant is smaller than 16 k_BT, that of water is 10 k_BT. Thus, for A_{PP} the Hamaker constant of the hydrated PEI/PEI layer we use the value 13 3 k_BT.[16] A_{SS}, the Hamaker constant of Silica/Silica equals 16.09 k_BT.[20] All Hamaker constants are expressed in units of k_BT at room temperature (4.0710^{-21}J).

Using the measured value for the force difference of 75 5 mN m^{-1} (see Figure 3; Section 3, Supporting Information), Equations (5) and (6) yield the value of the Hamaker constant of GO/Silica of 124.6 16.6 k_BT (Section 7, Supporting Information). This result is well reproduced when choosing different locations on the sample and when doing the experiment at different temperature and humidity as demonstrated in Figure 3d–f.

As a conclusion, on one hand, we found that 2D materials can be used as a nanometer-scale spacer, with sub-nm accuracy. On the other hand, we demonstrated that mimicking a "vacuum spacer" is possible in AFM force measurements. This leads to an accurate determination of the Hamaker constant between GO and silica, which is crucial to many GO based applications. This "vacuum-spacer method," that was in this paper applied to GO, can in principle be applied to other 2D materials as well. We believe that this will open new applications of 2D materials in nanoscience and nanotechnology.

Experimental Section

Chemicals and Materials: GO, synthesized using Hummer's method, was purchased from Graphene Supermarket. The elemental composition

of GO was characterized using X-ray photoelectron spectroscopy (Section 5, Supporting Information). A stable dispersion of 0.5 g GO in 1 L Milli-Q water was prepared using ultrasonication for 1 h, using an USC-TH ultrasonic bath from VWR Scientific. The dispersion was then centrifugation at 4000 rpm for 1 h, using a Megafuge 2.0R centrifuge from Heraeus Instruments with rotor radius of 20 cm. The supernatant was decanted and used for the sample preparation. Polyethylenimine (PEI, $M_w = 25\,000$ g mol^{-1}) was purchased from Sigma-Aldrich and used as received. A 0.1 g L^{-1} PEI aqueous solution was prepared using milli-Q water. A chip of about of 1 cm × 1 cm was cut from a (100) Silicon wafer with a native oxide layer of about 2 nm obtained from Sil'Tronix Silicon Technologies. The silicon chip was first rinsed with demi-water and ethanol followed by sonication using ethanol and acetone for 5 min, respectively. Plasma treatments of samples were performed with oxygen plasma for 1 min at a pressure of 1600 mTorr using a Harrick plasma cleaner (Anadis Instruments). After plasma treatment, the silicon wafer was stored in milli-Q water for more than 24 h to equilibrate.

Sample Preparation: The Si surface was coated with a monolayer of PEI by dipping the Si chip in an aqueous PEI solution (0.1 g L^{-1}) for 15 min. The sample was then rinsed in milli-Q water for 5 min to remove nonadsorbed PEI. Subsequent coating by GO was done by immersing the sample for 15 min in the aqueous GO dispersion prepared as described above. To remove excess GO, the sample was dipped in milli-Q water for 5 min. Due to carboxyl groups, GO is negatively charged and adsorbs at the positively charged PEI layer. All these steps in the sample preparation were done while the solution was stirred.

After deposition, a tape treatment was performed. The tape was pressed onto the sample using a finger as shown in inset of Figure 2b, and then torn off. To remove the polymer (PEI and/or residue of the tape treatment), the sample was treated with oxygen plasma for 1 min. This completes the sample preparation.

Instrumentation and Methods: A NTEGRA AFM instrument from NT-MDT was used in all AFM experiments. High sensitivity measurements were performed using the "HybriD Mode" method, developed and implemented by NT-MDT. This method combined height imaging and tip-sample force tracking simultaneously.[22] With hybrid mode AFM, a vertical oscillation of the sample was implemented at frequencies well below the resonances of the probe and the piezoelement to improve the signal to noise ratio. In the HybriD Mode method, at each point the tip performed a cycle of approaching and retracting. The range of approaching and retracting was set at 20 nm. In the approaching phase, the tip goes from nontouching to the touching regime, and the deflection signal of the cantilever records the force that the tip experiences. In the retracting phase of the cycle, the tip experiences strong adhesive interactions reflected by a jump by which the tip detaches. The latter jump is proportional to the magnitude of the adhesive force F. As a result, the surface morphology height image as well as the normalized adhesion-force image were obtained at the same time.

A NSG 03 silicon tip purchased from NT-MDT, with nominal value for the tip radius of 7 nm (guaranteed < 10 nm) and a nominal spring constant of 0.4–2.7 N m^{-1} was used with the hybrid mode measurements. Using high-resolution SEM, it was determined that the tip radius equals 10.6 nm (Section 6, Supporting Information). The actual value of the spring constant was measured using the thermal noise method.[23] Scanning the surface morphology, 512 × 512 points were recorded in 4 µm × 4 µm area. HA_NC AFM probes from NT-MDT with a silicon tip radii of about 10 nm were used for the standard tapping mode height scanning. The HybriD Mode images and standard tapping mode height images were all scanned with a rate of 0.5 Hz.

Supporting Information

Supporting Information is available from the Wiley Online Library or from the author.

Acknowledgements

The authors acknowledge the PhD Scholarship of Liangyong Chu from the China Scholarship Council of the Ministry of Education of China. The authors acknowledge Marcel Bus for the assistance with the AFM instruments.

Received: May 31, 2016
Revised: September 1, 2016
Published online: December 22, 2016

[1] A. K. Geim, I. V. Grigorieva, *Nature* **2013**, *499*, 419.
[2] a) D. R. Ward, N. K. Grady, C. S. Levin, N. J. Halas, Y. Wu, P. Nordlander, D. Natelson, *Nano Lett.* **2007**, *7*, 1396; b) D.-K. Lim, K.-S. Jeon, H. M. Kim, J.-M. Nam, Y. D. Suh, *Nat. Mater.* **2010**, *9*, 60; c) H. Li, Z. Song, X. Zhang, Y. Huang, S. Li, Y. Mao, H. J. Ploehn, Y. Bao, M. Yu, *Science* **2013**, *342*, 95.
[3] J. Sun, L. He, Y.-C. Lo, T. Xu, H. Bi, L. Sun, Z. Zhang, S. X. Mao, J. Li, *Nat. Mater.* **2014**, *13*, 1007.
[4] K. S. Novoselov, A. K. Geim, S. Morozov, D. Jiang, Y. Zhang, S. Dubonos, I. Grigorieva, A. Firsov, *Science* **2004**, *306*, 666.
[5] a) S. Stankovich, D. A. Dikin, G. H. Dommett, K. M. Kohlhaas, E. J. Zimney, E. A. Stach, R. D. Piner, S. T. Nguyen, R. S. Ruoff, *Nature* **2006**, *442*, 282; b) T. Ramanathan, A. Abdala, S. Stankovich, D. Dikin, M. Herrera-Alonso, R. Piner, D. Adamson, H. Schniepp, X. Chen, R. Ruoff, *Nat. Nanotechnol.* **2008**, *3*, 327; c) T. Kuilla, S. Bhadra, D. Yao, N. H. Kim, S. Bose, J. H. Lee, *Prog. Polym. Sci.* **2010**, *35*, 1350.
[6] G. Eda, G. Fanchini, M. Chhowalla, *Nat. Nanotechnol.* **2008**, *3*, 270.
[7] a) A. Das, S. Pisana, B. Chakraborty, S. Piscanec, S. Saha, U. Waghmare, K. Novoselov, H. Krishnamurthy, A. Geim, A. Ferrari, *Nat. Nanotechnol.* **2008**, *3*, 210; b) F. Schedin, A. Geim, S. Morozov, E. Hill, P. Blake, M. Katsnelson, K. Novoselov, *Nat. Mater.* **2007**, *6*, 652.
[8] S. F. Shi, F. Wang, *Nat. Nanotechnol.* **2014**, *9*, 664.
[9] Y. Li, Y. Wu, *J. Am. Chem. Soc.* **2009**, *131*, 5851.
[10] D. R. Dreyer, S. Park, C. W. Bielawski, R. S. Ruoff, *Chem. Soc. Rev.* **2010**, *39*, 228.
[11] H. Hamaker, *Physica* **1937**, *4*, 1058.
[12] J. Visser, *Adv. Colloid Interface Sci.* **1972**, *3*, 331.
[13] a) S. P. Koenig, N. G. Boddeti, M. L. Dunn, J. S. Bunch, *Nat. Nanotechnol.*, **2011**, *6*, 543; b) S. R. Na, J. W. Suk, R. S. Ruoff, R. Huang, K. M. Liechti, *ACS Nano* **2014**, *8*, 11234.
[14] J. Rafiee, X. Mi, H. Gullapalli, A. V. Thomas, F. Yavari, Y. Shi, P. M. Ajayan, N. A. Koratkar, *Nat. Mater.* **2012**, *11*, 217.
[15] J. Gregory, *J. Colloid Interface Sci.* **1981**, *83*, 138.
[16] J. Lyklema, *Fundamentals of Interface and Colloid Science, Volume 1: Fundamentals*, Elsevier, **1991**.
[17] a) H. Hamaker, *Recl. Trav. Chim. Pays-Bas* **1936**, *55*, 1015; b) H. Hamaker, *Recl. Trav. Chim. Pays-Bas* **1937**, *56*, 3; c) J. De Boer, *Trans. Faraday Soc.* **1936**, *32*, 10.
[18] S. Saito, T. Motokado, K. J. Obata, K. Takahashi, *Appl. Phys. Lett.* **2005**, *87*, 234103.
[19] X. Xiao, L. Qian, *Langmuir* **2000**, *16*, 8153.
[20] R. Hunter, *Foundations of Colloid Science*, Oxford:Claredon, New York, USA **1987**, 244.
[21] D. C. Marcano, D. V. Kosynin, J. M. Berlin, A. Sinitskii, Z. Sun, A. Slesarev, L. B. Alemany, W. Lu, J. M. Tour, *ACS Nano* **2010**, *4*, 4806.
[22] S. Magonov, NT-MDT Development Inc. http://www.ntmdt.com/hybrid-mode-afm, (accessed December 2016).
[23] R. Levy, M. Maaloum, *Nanotechnology* **2002**, *13*, 33.

